# Effective Brain Connectivity for fNIRS with Fuzzy Cognitive Maps in Neuroergonomics

Mehrin Kiani[1], Javier Andreu-Perez[2], Hani Hagras[1], *Fellow, IEEE*, Elpiniki I. Papageorgiou[3], Mukesh Prasad[4] Chin-Teng Lin[4], *Fellow, IEEE*

***Abstract*—Effective connectivity (EC) amongst functional near-infrared spectroscopy (fNIRS) signals is a quantitative measure of the strength of influence between brain activity associated with different regions of the brain. Evidently, accurate deciphering of EC gives further insight into the understanding of the intricately complex nature of neuronal interactions in the human brain. This work presents a novel approach to estimate EC in the human brain signals using enhanced fuzzy cognitive maps (FCMs). The proposed method presents a regularized methodology of FCMs, called effective FCMs (E-FCMs), with improved accuracy for predicting EC between real, and synthetic fNIRS signals. Essentially, the revisions made in the FCM methodology include a more powerful prediction formula for FCM combined with independent tuning of the transformation function parameter. A comparison of EC in fNIRS signals obtained from E-FCM with that obtained from standard FCM, general linear model (GLM) parameters that power Dynamic Causal Modelling (DCM), and Granger Causality (GC) manifests the greater prowess of the proposed E-FCM over the aforementioned methods. For real fNIRS data, an empirical investigation is also made to gain an insight into the role of oxyhemoglobin and deoxyhemoglobin (oxy-Hb, deoxy-Hb) in representing the cognitive activity. We believe this work has profound implications for neuroergonomics research communities.**

***Index Terms*—Fuzzy connectivity measures, Brain connectivity, Effective Connectivity, Fuzzy Cognitive Maps, Functional Neuroimaging**

## I. Introduction

An *effective connectivity* (EC) amongst the brain signals represent influence between neural systems which can be both activity, and/or time dependent [1], [2]. Hence EC elucidates the relationships in a brain network thus formed during a cognitive task undertaken by a subject. An accurate deciphering of connections amongst the brain signals is a significant step towards a better understanding of EC linkages between different brain regions. A comprehensive picture of EC between brain regions, for a particular mental task, can lead to a thorough assimilation of the workings of the human brain [3]. Owing to the significance associated with the detection and subsequent analysis of the discerned influence between brain regions, an accurate interpretation of EC in fNIRS data is crucial.

Owing to the multitude of advantages of functional near-infrared spectroscopy (fNIRS) over functional magnetic resonance imaging (fMRI) such as the former being safe, cost efficient, and a portable technique with reasonable spatial and excellent temporal resolution, fNIRS is fast replacing fMRI for empirical studies in the field of neuroscience. This is true in particular for psychological studies where brain activity is inspected to understand human factors at work and normal life settings. This new paradigm of research has been termed as *Neuroergonomics* [3].

The de facto standard for EC analysis in fMRI studies is Dynamic Causal Modelling (DCM) [4]. However DCMs cannot be used for discerning EC in fNIRS data since the temporal resolution of fNIRS is sufficient to be affected by interregional axonal conduction delay [5]. This is because extending DCMs to account for time delays will not only introduce parameterized complexity but also pose a problem of formulation. In this regard, an alternative approach that is used to estimate connections in fNIRS data is Granger Causality (GC) [6]. The GC is a relatively fast, scalable technique that can be used to compute EC while taking into account time delays. However, GC analysis cannot transcribe non-linear cause-effect relationships without compromising GC scalability owing to the linear vector auto regression in GC [6], [7].

The GC analysis is also predominantly dependent on the pertinent information presented beforehand. Essentially it implies that the GC analysis may identify spurious connections, or even estimate wrong feedback relations [8] on account of missing relevant information. Further, the limitations of GC analysis comprise its inability to account for connections that change direction over time [8]. Another consequential constraint that limits GC analysis applicability is its dependence on the temporal resolution in the data to be analyzed for accurate deciphering of EC. Hence if the data has low temporal resolution than the minimum resolution to identify the time lags between which an influence transpires, the GC analysis will not be able to decipher the underlying EC in the data [9].

In the realm of neuroimaging, and in particular for fNIRS data, the sensitivity of GC analysis to the lack of relevant information is critical. Essentially, it renders the inference made by GC rather obscure for identification of EC in fNIRS data. Moreover, the GC analysis is unable to transcribe nonlinear effective connections and is also unable

[1,2]Computational Intelligence Centre, School of Computer Science and Electronic Engineering, University of Essex, United Kingdom
[2]Faculty of Medicine, Imperial College London, United Kingdom
[3]Department of Electrical Engineering, University of Applied Sciences (Technological Education Institute) of Thessaly, Larisa, Greece
[3]Department of Computer Science, University of Thessaly, Papasiopoulou 2-4, Lamia, 35100, Greece
[4]CIBCI Lab, Centre for Artificial Intelligence, FEIT, University of Technology Sydney, Australia

to assimilate effective links changing direction over time. This has implications for GC application in fNIRS data since the underlying EC in fNIRS data are inherently non-linear. Furthermore, the lack of flexibility of GC to cater for changing effective connections renders GC particularly inapplicable for an insightful EC analysis between fNIRS data. Owing to the aforementioned shortcomings of GC analysis for uncovering the EC in fNIRS data in particular, we propose the novel approach of using Fuzzy Cognitive Maps (FCMs) to delineate EC in fNIRS data.

The major four contributions of the proposed methods are as follows: 1) An automatic data driven method is proposed to compute EC from neural hemodynamic data. 2) A new FCM formulation, called Effective Fuzzy Cognitive Maps (E-FCMs), for regularizing the network by weight reinforcement using error-driven learning. 3) E-FCM fusion from individual E-FCMs obtained from bidimensional hemodynamic data. 4) An empirical analysis of the individual contribution of oxy-Hb and deoxy-Hb in representing the underlying cognitive activity. In particular, this work presents an approach at fusion of bi-dimensional fNIRS data whilst retaining their individualism by utilizing individual E-FCM models representative of EC generated by both oxy- and deoxyhemoglobin (oxy-Hb, deoxy-Hb). This approach has the potential for uncovering the EC in fNIRS data more accurately since it explores its dual dimensions both separately at first, and then by combination later.

## II. High-Order Fuzzy Cognitive Maps

An FCM is inherently a signed directed fuzzy graph which is capable of representing *fuzzy connectivity* between variables as fuzzy degrees of relationships in a complex system. The advantages of FCMs over GC analysis are numerous owing to their expressiveness, and flexibility they inherit from neuro-fuzzy systems. FCMs are scalable, can handle non-linear data, and combined with their prowess to accommodate changing effective connections along with the flexibility to modify the memory order of the model, they offer a powerful paradigm to analyze EC in fNIRS data. The extension of the generic FCM model to a higher-order memory implies that those complex systems, such as fNIRS data, which exhibit higher-order effective connections amongst their concepts can also be modelled by FCM [10], [11].

FCMs offer a graphical representation of the dynamics of a given system which can be seen as a combination of fuzzy logic, and neural networks [10]. FCMs are widely recognized for discerning the presence, and strength of relationships between nodes in a given dynamic system from various domains such as engineering, medicine, control, and political affairs [12]–[16].

Following is a formal mathematical description of a higher order FCM [15]:

$$C_j(t+1) = f(\sum_{l=0,l\leq t}^{k}(g_j(l)\sum_{i=1}^{N}e_{ij}C_i(t-k))) \quad (1)$$

where $C_j(t)$ is the fuzzy value of the concept or node (or signal in fNIRS paradigm) $j$ at time $t$ based on the strength of the interaction, $e_{ij}$ in the range $[-1, 1]$, of concept $j$ with other concepts in the system, and the past values of the concept $j$, $C_j(t-k)$. The total number of concepts in a given system is represented by $N$ and $T$ denotes the total length of a signal. The number of past fuzzy values of a given concept to be considered by the FCM when computing the new fuzzy value for that concept is dictated by the order of the FCM, represented by $k$. The FCM also allows for tuning the strength of influence of the preceding fuzzy values on the current fuzzy value for a given concept by optimizing values of $g_j(k)$, and $e_{ij}$ using Genetic Algorithm (GA).

The new fuzzy value for a given concept is normalized using a transformation function with a specified normalized range. The most commonly used tranformation function is the sigmoid function (2) that restricts the weighted sum to the usual range of $[0, 1]$ [17], [18]. The transformation function $f(x)$, used in this work (3), is inherently a sigmoid function with range of $[-1, 1]$. This normalization of fuzzy degree of relationship of a particular concept with respect to any other concept in the fuzzy graph facilitates the comparative analysis such that a value of 1 means fully interconnected, a value of -1 means fully interconnected in the opposite direction, a value of 0 means disconnected, and a value between 0 and 1 (or -1) means interconnected to a certain extent.

$$sigmoid(x) = \frac{1}{1+e^{-Cx}} \quad (2)$$

$$f(x) = 2sigmoid(2x) - 1 \quad (3)$$

where $C$ is a parameter used to define a particular shape of the sigmoid function. The most common value of $C$ found in literature is 5 [14], [19].

A quantitative assessment of the predicted states generated by the FCM can be done using the two standard FCM error functions Error 1 and Error 2 outlined in (4) and (5) [14], respectively. The error is estimated by comparing the reconstructed signals from the resultant FCM model with the original signals- synthetic fNIRS signals for Experiment 1, and real fNIRS signals for Experiment 2.

$$error_1 = \sum_{t=1}^{T}\sum_{i=1}^{N}|C_i(t) - \hat{C}_i(t)| \quad (4)$$

$$error_2 = \sum_{t=1}^{T}\sum_{i=1}^{N}|(C_i(t) - \hat{C}_i(t))^2 + (C'_i(t) - \hat{C'}_i(t))^2| \quad (5)$$

where $\hat{C}$ is the predicted state of the concept of resultant FCM, and $C'$ is the rate of change in the state of a concept.

## III. Related Works

### A. EC in fNIRS

One of the most common approaches for computing EC in fNIRS data is through GC analysis. The work by Holper *et al.* [20] focus on computing EC via GC between brain signals recorded from two subjects undertaking the same task simultaneously. They conclude that GC values are greater for

signal of the model to cause the imitator signal than when the direction is reversed i.e. from the signal of the imitator to that of the model. This could be attributed to the limitation of the GC model to read the causality within the same set of signals when the direction and/or time lag during which causality transpires is changed. In the study by Im *et al.* [21], the fNIRS signal analysis is conducted using GC. Their conclusion is also limited to unidirected coupling between the somatosensory areas and the motor areas, owing to limitations imposed by unidirectional data analysis of GC.

A comparative study of the brain activity recorded during rest and movement using fNIRS is done by Bajaj *et al.* [22]. The estimation of EC in the recorded fNIRS data is done by GC. However, they credited the use of DCM over GC analysis when there is varying time lag in activation of causation between two signals. This is due to limited prowess of GC to analyze signals with time lag, or the order of causality, unknown and/or varying. An interesting study by Yuan [23] presents estimating EC by using GC mapping on regions of interest (ROIs) identified by independent component analysis (ICA). The improved results of the GC-ICA hinges on accurate over simplification of the brain regions identified by ICA along with the associated shortcomings of GC analysis for fNIRS data.

An attempt to estimate EC using DCM is done by Tak *et al.* [5]. Though their results are consistent with findings of the previous fMRI studies, successful application of DCM for EC analysis on fNIRS data is highly contingent on the undertaken task and hence the corresponding characteristic hemodynamic response function used in DCM analysis.

### *B. Learning Methods for FCMs*

A hybrid technique for FCMs learning for predicting nonstationary time series is proposed by Yang *et al.* [24]. They present the use of wavelet transform with higher order FCMs for predicting nonstationary time series. The application of wavelet transform converts original time series into multivariate time series, which are then employed by higher order FCMs to model, and predict the original nonstationary time series.

Towards automatic learning of large scale FCMs the work by Zou *et al.* [25] presents the use of mutual information based two phase memtic algorithm (MA). Their work optimizes the edge weights of only those links identified in the first phase of MA, thereby reducing the search space for MA. The works by Wu *et al.* offer two different approaches for large-scale and sparse FCMs learning, one using compressed sensing [26] and the second using least absolute shrinkage and selection operator [27].

The use of multiagent genetic algorithm for large scale FCMs learning is done by Liu *et al.* [28]. Their work demonstrates the strength of using multiagent genetic algorithm for reconstructing large scale gene regulatory networks with 200 nodes.

### *C. Pruning Methods for FCMs*

A critical problem in the simulation of computational networks, like FCMs and artificial neural networks (ANNs), is over fitting due to a large number of learnable parameters introduced to accurately model a given system [29]. Amongst the prominent works done for regularization of neural networks to minimize overfitting include DropOut (DO) [30], and DropConnect (DC) [31]. In DO [30], nodes (along with any associated connections) from the hidden and/or output layer(s) are dropped out randomly during training. Whereas in DC [31] only some of the connections are randomly removed rendering DC to be a more liberal form of network regularization than DO. Both works demonstrate a higher network performance post implementation of network regularization.

One noteworthy solution for the pruning of FCM specifically is proposed by Averkin [18]. In their work, a regularization of FCMs for hybrid decision support system is presented. The work proposes pruning of weights as an approach to compensate for 1) expert inaccessibility for modelling a system that vary a little from their experience, and 2) multiple experts to collaborate on one system. The work is limited by the assumption that the system model does not change during the course of the analysis.

Another consideration in FCMs implementation is the normalization of weights using a transformation function to a certain specified range (usually [0,1] for FCMs). The steepness or the gradient of the transformation function establishes the range of variability of the non-normalized weights that will have non-extreme (neither 0 nor 1) normalized equivalents. In essence, the parameter tuning defines the window of the non-normalized weights that can contribute meaningfully to the model estimation by a FCM simulation.

In this regard, the work by Papageorgiou and Froelich [17] is a significant contribution towards the transformation function parameter optimization. The study investigates the influence of the transformation function parameter on the shape and properties of the transformation function. They conclude that optimization of the transformation function parameter is quintessential for the FCM model to fit a given data set.

## IV. Materials and Methods

### *A. fNIRS Data*

fNIRS is a popular neuroimaging technique used extensively for the study of brain activity. It is capable of recording brain activity in real time by detecting changes in metabolic profile of a given brain region under investigation. The changes in concentration of oxy-Hb, deoxy-Hb can be inferred from metabolic activity and oxygen consumption of the underlying neural tissues [32], [33]. The recorded hemodynamic response can be used in the study of neuroergonomics, and brain computer interfaces [34]. Since fNIRS has a multitude of advantages over other neuroimaging techniques (eg. fMRI) such as it is low-cost, offers better temporal resolution, has a higher sampling rate, and robustness to motion artifacts alongside safety, and portability, fNIRS is fast becoming a medium of choice for empirical investigations in cognitive neuroscience [35], [36].

In this section, a description of synthetic [32] and real fNIRS [36] data used to evaluate the proposed E-FCM methodology for detecting EC is presented.

*1) Experiment 1:* In this work synthetic fNIRS data is generated to evaluate the efficacy of the proposed E-FCM methodology for assessing EC in fNIRS signals. The method outlined by Scarpa *et al.* [32] is reproduced to generate a total of 16 synthetic fNIRS causal signals. The synthetic fNIRS signals are generated according to (6), with minor modifications to accommodate the needs of this work:

$$y_{sim}(t) = k u_{true}(t) + 0.01\phi_{sim}(t) + \eta(t) + r(t) \quad (6)$$

where $u_{true}(t)$ represents the true hemodynamic response (HR). The true HR, $u_{true}(t)$, is scaled by a constant $k$ which can take the value of 0, 0.5 or 1. The channel location would determine the exact value of $k$ for a given synthetic fNIRS signal. The processes of physiological noise, random noise, and noise due to possible motion artefacts are represented by $\phi_{sim}(t)$, $\eta(t)$, and $r(t)$ respectively in the overall simulated fNIRS signal, $y_{sim}(t)$.

For more information on $u_{true}(t)$, and noise models in (6), the reader is referred to [32], [37], [38].

Fig. 1 shows a representative synthetic fNIRS signal, $y_{sim}(t)$, corresponding to a given true HR stimulus, $u_{true}(t)$. The synthetic fNIRS signal is inherently noisier than true HR stimulus by contributions from physiological and random noise mainly. The incorporation of physiological noise also stretches the length of the HR stimulus in the synthetic fNIRS whilst the occurrence of the maximum displacement of the synthetic fNIRS is in sync with that of the true HR stimulus [38]. A total of 16 synthetic fNIRS signals are generated to remain consistent with the 16 real fNIRS signals available as outlined in section IV-A2.

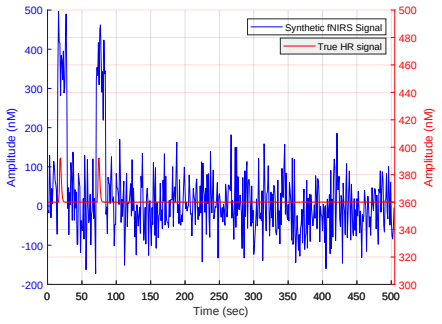


Fig. 1: Synthetic fNIRS signal (blue) generated by the corresponding true HR signal (red).

*a) Preprocessing of Synthetic fNIRS data:* Inherently, fNIRS signals are a measure of the metabolic changes in the blood owing to cognitive activity. In this regard, motion artefacts arising from possible head movement can cause fluctuations in fNIRS recordings which are not representative of the cognitive activity. Therefore, it is crucial to remove motion artefacts from fNIRS signals before analyzing it for more accurate assessment of cognitive activity in the brain.

In this work, the synthetic fNIRS signals are filtered using Kalman filter as outlined in [39]. The order of the state space model is one, and the autoregressive model parameters are estimated using the Yule-Walker equations.

The filtered synthetic fNIRS signals are also down sampled before introducing EC within the data. This is because the total length of the synthetic fNIRS signal ($\approx$ 500 s) is significantly larger ($\approx$10 times) than the length of the signal where the two true HR stimulus transpire ($\approx$50 s) hence down sampling the signal will pronounce the connectivity within the data by omitting some non-salient data points. In this work the down sampling factor is experimentally chosen to be 10 such that the fNIRS data still retains its characteristics.

*b) Effective Synthetic fNIRS connectivity data:* The EC in the down sampled and filtered synthetic fNIRS data is incorporated according to Fig. 2 and (7) [40]. As can be seen in Fig. 2 and (7), signal 1 ($X_t^1$) value at time $t$ is independent of all other signals. However, signal 2 ($X_t^2$) and signal 3 ($X_t^3$) value is dependent on signal 1 ($X_{t-2}^1$) value with a time lag of 2, and signal 1 value with a time lag of 3 ($X_{t-3}^1$) respectively. The signal 4 ($X_t^4$) values is influenced by signal 1 values ($X_{t-1}^1$) and ($X_{t-2}^1$), and signal 5 ($X_{t-1}^5$) values; whereas only signal 4 ($X_{t-1}^4$) influences on signal 5 ($X_t^5$).

The 16 synthetic fNIRS signals are enhanced with EC by forming three sets of five signals each having same dependencies as delineated in Fig. 2 and (7). The 16th signal (like the 1st, 6th, and 11th signal) has no causal dependencies on any other signal(s). A generic connection matrix, $E$, with elements $e_{ij}$, corresponding to the causal network illustrated in Fig. 2, and (7) is shown in Table I.

The resultant set of 16 synthetic fNIRS signals enhanced with EC is used by the E-FCM model to estimate the EC within the signals.

$$\begin{cases} X_t^1 = X_t^1 + 0.95\sqrt{2}X_{t-1}^1 - 0.9025X_{t-2}^1 \\ X_t^2 = X_t^2 + 0.5X_{t-2}^1 \\ X_t^3 = X_t^3 - 0.4X_{t-3}^1 \\ X_t^4 = X_t^4 - 0.5X_{t-2}^1 + 0.25\sqrt{2}X_{t-1}^4 + 0.25\sqrt{2}X_{t-1}^5 \\ X_t^5 = X_t^5 - 0.25\sqrt{2}X_{t-1}^4 + 0.25\sqrt{2}X_{t-1}^5 \end{cases} \quad (7)$$

*2) Experiment 2:* The real fNIRS data [36] used in this work comes from a Neuroergonomics study that involved 27 right-handed male surgeons affiliated with National Health Service, and Imperial College London.

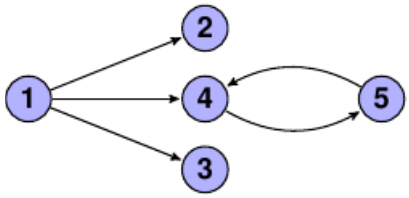


Fig. 2: EC between synthetic fNIRS signals: signal 1 is influencing signals 2, 4, and 3, whereas signal 4 and signal 5 are influencing each other.

TABLE I: Generic connection matrix, $E$, for causal network shown in Fig. 2, and (7)

| Concepts | $\mathbf{X_1}$ | $\mathbf{X_2}$ | $\mathbf{X_3}$ | $\mathbf{X_4}$ | $\mathbf{X_5}$ |
|---|---|---|---|---|---|
| $\mathbf{X_1}$ | 0 | $e_{12}$ | $e_{13}$ | $e_{14}$ | 0 |
| $\mathbf{X_2}$ | 0 | 0 | 0 | 0 | 0 |
| $\mathbf{X_3}$ | 0 | 0 | 0 | 0 | 0 |
| $\mathbf{X_4}$ | 0 | 0 | 0 | 0 | $e_{45}$ |
| $\mathbf{X_5}$ | 0 | 0 | 0 | $e_{54}$ | 0 |

A local research ethics committee approval was obtained (project number: 05/Q0403/142). The participants performed a complex visual-spatial task (namely laparoscopic surgery (LS)) whilst their brain activity is recorded, as shown in Fig. 3. Specifically, amongst the 27 surgeons included 9 novices (NV), 10 trainees (TN), and 8 expert (EX) consultants. The reader is referred to [36] for a more detailed description of the participants, the task, and the pre-processing of the fNIRS signals.

A total of 16 real fNIRS signals are used in this study. The fNIRS digitized probe positions were registered from a real-world coordinate to the Montreal Neurological Institute (MNI) space. The MNI coordinates were transformed to Talairach space [41], and look up in a brain atlas [42] to establish their relations with the ROI. A detailed explanation of the fNIRS probe positions transformation is provided in the study by Andreu-Perez *et al.* [36]. The measured channels locations are as shown in Fig. 4.

The reason this particular dataset is chosen to gauge the performance of E-FCM method is because the participants can be categorized based on their expertise level for performing LS. A range of expertise within the participants implied a better differentiation can be inferred in the cognitive activity arising from the dexterity of the task.

The dataset also entails separate records for oxy-Hb and deoxy-Hb levels in the investigated brain regions. Hence, in order to better assess the EC within the 16 real fNIRS signals grouped using the proposed E-FCM model, the oxy-Hb fNIRS signal and deoxy-Hb fNIRS signals are analyzed separately. This is important because no direct coupling of the two hemoglobin dimensions of fNIRS has been established in the literature yet [33], [43], [44] therefore it would be counter-intuitive to use total hemoglobin (THb) response

Fig. 3: Brain activity being recorded via fNIRS whilst participants perform LS task.

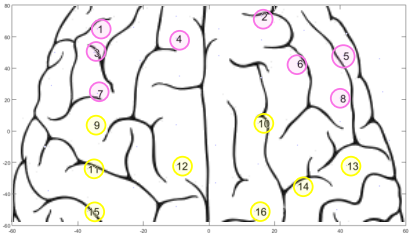


Fig. 4: The 16 measured fNIRS signals channel position differentiated based on ROIs- Prefrontal Cortex (PFC) in pink, and Motor Cortex (MC) in yellow.

instead of individual hemoglobin responses. However, the discrepancies between the oxy-Hb and deoxy-Hb signal may be meaningful to elucidate transient neural activity as revealed in Sasai *et al.* [45]. A detailed discussion of how the dual dimensionality of fNIRS signals has been used in this work to establish EC in the brain regions is presented in following sections: IV-A2a and IV-D.

*a) Fusing Hemodynamic Varieties:* In order to address the particular issue of which hemoglobin response is more representative of the metabolic activity in the underlying neural tissue, the individual effective links deduced by the E-FCM model for both hemoglobin dimensions of fNIRS are analyzed separately and used to compute an overall network that is a combination of the stand-alone networks of oxy-Hb and deoxy-Hb signals.

In particular, the resulting weights of the connection matrix from the E-FCM simulation of both oxy-Hb and deoxy-Hb for all NVs, TNs, and EXs are averaged based on their accuracy level as outlined in section IV-D. This would facilitate minimization of any random errors that may arise due to slight environmental changes whilst recording of the data as well as any discrepancies within the subjects per category (such as intelligence quotient (IQ), degree of alertness etc.). The averaged weights of the oxy-Hb and deoxy-Hb are then analyzed to compute an overall E-FCM representing both dimensions of fNIRS. In essence, the combined E-FCM would be a representative of the THb response without undermining the individual characteristics of both oxy-Hb and deoxy-Hb.

### *B. Effective Fuzzy Cognitive Maps (E-FCMs)*

In this section, the proposed changes to the FCM are outlined. These revisions include a regularized FCM prediction formula motivated from DC for neural networks [31], optimization of the transformation function parameter value, $C$ in (2), and the significance of employing a higher order FCM, $k$ in (1), in particular for detecting EC in fNIRS signals.

The proposed regularization of FCM is achieved by straining the weights of the connection matrix, $E$, using a soft regularizer, $Z$. The soft regularizer $Z$ is a generalization of DC mask since elements of $Z \in \mathbb{R}$ and can attain any value in the range of $[0, 1]$ unlike a binary mask in DC whose elements can only be 0 or 1 [31]. The elements in $E$ and $Z$ are both optimized using GA, however, please note only elements of $E$ can model the direction of the EC whereas $Z$ can only

optimize the strength of the EC, and hence cannot affect the direction of EC unlike $E$.

Eq. (8) entails the formal mathematical definition of E-FCM:

$$C(t+1) = f(g; (E \odot Z)C(t))$$
$$C_j(t+1) = f(\sum_{l=0, l\leq t}^{k} (g_j(l) \sum_{i=1}^{N} (e_{ij} \odot z_{ij}) C_i(t-k))) \quad (8)$$

where $C_j(t)$ is the fuzzy value of the concept or node (or signal in fNIRS paradigm) $j$ at time $t$ based on the strength and direction of the interaction, $e_{ij} \odot z_{ij}$ ($\odot$ represent element wise multiplication) in the range $[-1, 1]$, of concept $j$ with other concepts in the system, and the past values of the concept $j$, $C_j(t-k)$. The total number of concepts in a given system is represented by $N$ and $T$ denotes the total length of a signal. The number of past fuzzy values of a given concept to be considered by the E-FCM when computing the new fuzzy value for that concept is dictated by the order of the E-FCM, represented by $k$. The E-FCM also allows for tuning the strength of influence of the preceding fuzzy values on the current fuzzy value for a given concept by optimizing values of $g_j(k)$, $z_{ij}$, and $e_{ij}$ using GA.

The effectiveness of the E-FCM arises from entailing greater degrees of freedom owing to the weight regularizer $Z$ whilst finding the optimum EC direction, and strength without violating the set of constraints imposed (see tolerance criterion in section IV-C) on it. In the Results section V-A and in particular Fig. 7 and Table III, a comparison of E-FCM results with the original FCM results is also made to further fortify the effectiveness of E-FCM.

In this work, both Error 1 (4) and Error 2 (5), are computed when analyzing the performance of the proposed E-FCM technique for evaluating the effective connections between synthetic signals, and real fNIRS signals, separately.

*1) Transformation Function Parameter Tuning:* As mentioned earlier, transformation function is responsible for normalizing the fuzzy degrees of relationship (or weight values) in a specified range. The particular transformation function used in this work is the sigmoid function, see (3). Essentially, the gradient of the transformation function determines how fast the non-normalized fuzzy degrees of relationship are squeezed into the normalized range for the fuzzy degrees of relationship.

Fig. 5 shows the transformation function plot for two values of the parameter, $C$, that defines the gradient of the function. The value for $C$ is assumed to be 5 for most practical applications [14], [19]. However, with $C = 5$, the gradient of the transformation function proved too steep to suit the needs for this work- the fuzzy degrees of relationship were being squashed to the normalized range too fast, and hence were not generating the required results.

In contrast, the empirically found value of $C = 1$, is more inclusive of the non-normalized fuzzy degrees of relationship to be translated to the non-extreme values in the normalized range for the fuzzy degrees of relationship by having a less steep gradient. This can also be seen in Fig. 5. The transformation function with $C = 1$ (red) is including values from approximately $(-4, 4)$ to be converted to non-extreme normalized equivalents whereas with $C = 5$, values from the approximate range of $(-1, 1)$ only are being translated to non-extreme counterparts in the normalized fuzzy degrees of relationship.

*2) E-FCM Order, $k$:* The E-FCM order dictates how many past fuzzy values, $k$, in a set of observations will be considered by the E-FCM when trying to discern a fuzzy effective connection between them. The implications of the choice of the order of the E-FCM are largely dependent on the particular application. In (8), the parameter $k$ defines the order of the E-FCM. As is also evident in (8), the impact of the preceding state(s) on the current state can also be scaled by tuning the value of the parameter $g$.

The motivation for employing a higher order E-FCM for fNIRS signals lies in a more accurate deciphering of the fuzzy EC between the fNIRS signals. This is owing to complex, higher order fuzzy effective connections amongst the fNIRS signals which first order E-FCM dynamics cannot comprehend very well.

### C. E-FCM Learning

The E-FCM learning can be achieved either manually using the information provided by experts or by employing an automated process that can use historical information to develop FCMs [15]. There is an increasing trend to use computerized techniques to uncover the fuzzy relations between concepts for an FCM simulation [46] since using an automated approach to learn the inherent model of a given system does not introduce a bias in the FCM simulation that may be incorporated into the results had the FCM evolution been governed by human knowledge.

In accordance with the greater advantages of automated FCM learning, in this work, E-FCM learning is achieved by utilizing the GA. GA is an optimization algorithm that is based on evolutionary ideas of natural selection and genetics and is capable of solving both constrained and unconstrained optimization problems. Owing to its robust, and heuristic nature, GA can be applied to learn the inherent model of a given system using the historical data of the system [14].

The GA can also accommodate the learning of peculiar characteristics of a system by tuning its inherent parameters.

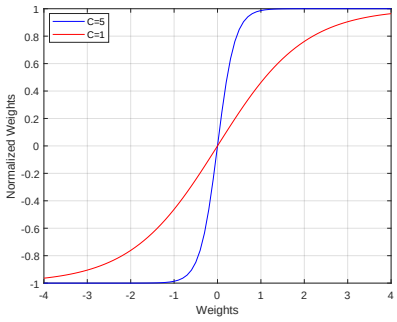


Fig. 5: Transformation function with $C = 5$ (blue) and $C = 1$ (red).

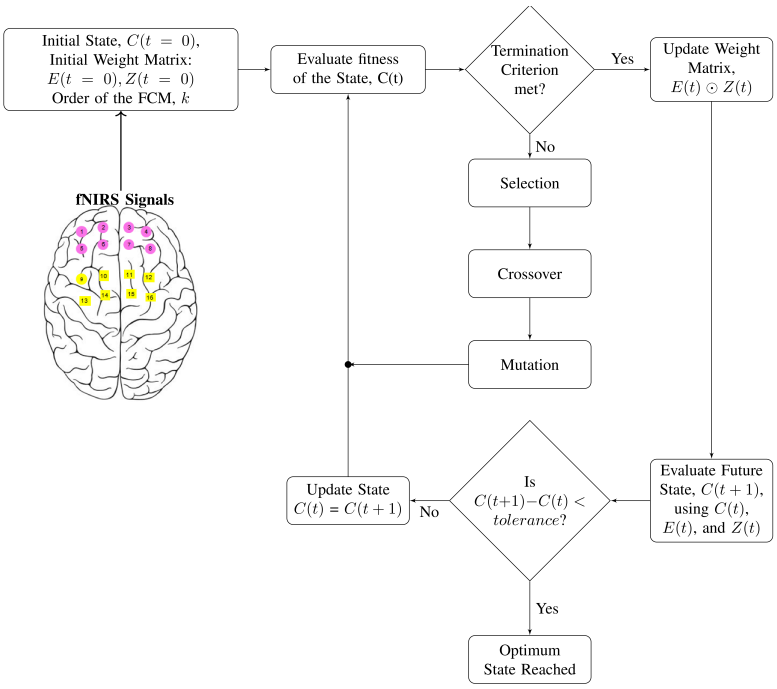


Fig. 6: A flowchart of the algorithm for predicting EC in fNIRS signals using the proposed E-FCM model.

In this work, the values of these parameters were empirically determined such that the resultant connectivity matrix, $E$, depicted the inherent structure of the 16 synthetic fNIRS signals as close as possible. The population size of the GA is set to 1000, the maximum number of generations is defined as 1000 x the population. The maximum fitness is set to 0.99 and the tolerance criterion is set to $1e^{-1}$. The genetic operator used is crossover and the selection is made by tournament. A detailed description of the GA parameters can be found in [14], and [46].

The flowchart in Fig. 6 outlines the steps for the generation of a resultant connection matrix, $E \odot Z$, by GA using historical data to be incorporated in the E-FCM simulation. The E-FCM builds the next state vector, $C(t+1)$, of a given system using the resultant connection matrix, $E \odot Z$, and the historical data, $C(t)$, till a chosen tolerance criterion is achieved.

The GA learning is driven by the *fitness* of the predicted state $\hat{C(t)}$ with respect to the original state $C(t)$. The fitness of the predicted state $\hat{C(t)}$ is evaluated according to the fitness function (9), $f$.

$$f = \frac{1}{10(T-1)N} error \tag{9}$$

where $T$ is the length of each of the total $N$ signals and the $error$ is computed using (5).

The fitness of each predicted state $\hat{C(t)}$ is gauged against an apriori termination criterion, and if achieved, the weight matrix $E(t) \odot Z(t)$ is updated accordingly, see Fig 6. In case the termination criterion is not met, the GA will try to look for new offsprings using selection, crossover, and mutation, to generate a new predicted state $\hat{C(t)}$ which will then again be compared with the termination criterion, and the process will continue to repeat itself till the chosen termination criterion is satisfied.

### D. E-FCM Fusion

The fNIRS channels locations, which are concepts/nodes for an E-FCM simulation, are identical for both oxy-Hb and deoxy-Hb, therefore the only facet that needs conformation for E-FCM combination is the connections between the concepts. Within the connections realm, the details that need assimilation are the presence/absence, positive/negative relation, and the strength (weight) of the fuzzy degrees of relationship between the channels. In this work, the strength of the fuzzy degrees of relationship in combined E-FCM for the case where a connection of the same polarity (negative or positive) is present in both oxy-Hb and deoxy-Hb E-FCMs is computed by taking the average of their respective fuzzy degrees of relationship in individual E-FCMs. For the case where a connection is present only in one of the parent E-FCMs, oxy-Hb or deoxy-Hb, it is included in the combined E-FCM with the same fuzzy degree of relationship as in the parent E-FCM. The last case where a connection is present in both E-FCMs albeit with different polarities, the overall E-FCM does not include it, the conflicting connection. A similar work for combining FCMs in group decision making is done by Hanafizadeh et al. in [12] where individual FCMs originating from different experts are consolidated to arrive at a FCM that represents the decisions of all the experts involved.

Owing to the absence of any established direct link between oxy-Hb and deoxy-Hb that confers the presence of brain activity [33] [43] [44], the approach of a merger E-FCM that reads from both oxy-Hb and deoxy-Hb E-FCM offers a greater accuracy into establishing the overall EC within

TABLE II: Total Error Values for different orders of E-FCM

| TOTAL ERROR | Order, $k$, of E-FCM | | | | |
|---|---|---|---|---|---|
| | 1 | 2 | 3 | 4 | 5 |
| **Error 1** | 30.89 | 41.28 | 21.59 | 37.92 | 28.10 |
| **Error 2** | 60.15 | 93.97 | 50.42 | 82.43 | 61.07 |

different regions of the brain. Hence, connections with the same polarity in the parent E-FCMs are corroborated, and connections present in any one of the parent E-FCM are retained, to bespeak the significance of EC transpiring between the corresponding channels. However, the connections which have opposing effective connections in the parent E-FCMs are inconclusive, and consequently removed from the overall E-FCM.

## V. Experiments and Results

### A. EC Computation on Synthetic fNIRS data

In order to assess the efficacy of the proposed E-FCM technique for evaluating the EC between 16 synthetic fNIRS signals, the reconstructed signals generated by third order E-FCM are compared with the reconstructed signals generated from standard FCM, the reconstructed signals from general linear model (GLM) parameters based on canonical hemodynamic response function (DCM-GLM) [47] [48], the reconstructed signals from bivariate linear autoregressive model [40] [49] that drives GC (GC-AR), and the original signals. A plot of the reconstructed signals from E-FCM (red) with reconstructed signals from standard FCM (green), GC-AR (cyan), and DCM-GLM parameters (black) are shown along with the original signals (blue) in Fig. 7. The Multivariate Granger Causality Toolbox (MVGC) [50] has been used to compute GC-AR parameters and DCM-GLM parameters are estimated using SPM-fNIRS toolbox [51].

A visual assessment of Fig. 7 indicates that the third order E-FCM is able to discern well the characteristic peaks, i.e. the true HR stimulus, for most of the synthetic fNIRS signals with effective connections. In contrast, as can also be seen in Fig. 7, a total of four predicted signals from standard FCM technique (shown in green) had no HR stimulus (Row (R) 1, Column (C) 4; R2, C1; R3, C4; R4, C2) at all. This is owing to overfitting in the absence of a weight regularizer $Z$ in the standard FCM formulation (1) to find the optimum weights whilst satisfying the set of constraints imposed on it. Likewise, the reconstructed signals from DCM-GLM parameters are unable to predict the second HR stimulus for almost all 16 signals.

The order, $k$, of the E-FCM is empirically chosen, third in this case, such that minimum possible values are attained by Error 1(4), and Error 2(5). The total error value, i.e. the sum of error for all 16 synthetic fNIRS signals, for Error 1 and Error 2 for different orders of E-FCM are reported in Table II. As can be seen in Table II, the total error values for both Error 1 and Error 2 are the least for E-FCM order $k = 3$.

A quantitative assessment of the third order E-FCM results is also done by computing values for Error 1(4), and Error 2(5), and comparing them with those obtained for standard FCM, GC-AR, and DCM-GLM results. The error values for all methods are tabulated in Table III. Since Error 2 also factors in the differences in the rate of change of the predicted values with the original values when computing the error hence Error 2 values are considerably larger than their corresponding Error 1 values. The average error values for E-FCM are the least when compared with GC-AR, DCM-GLM, and standard FCM average error values.

The performance of the proposed third order E-FCM is also gauged against the equivalent results obtained from GC. GC is a statistical tool and the de facto standard for evaluating future values of a time series variable ($Y$) from past values of both itself and another time series variable (X), if it is established that $X$ *Granger* causes $Y$ [40] [49]. The Multivariate Granger Causality Toolbox (MVGC) [50] has been used to compute the values of GC for the 16 synthetic fNIRS.

Fig. 8 shows a comparison of established EC using GC (Fig. 8 (b)) and proposed third order E-FCM (Fig. 8 (c)) with the true effective connections (Fig. 8 (a)). A filled black square connecting two signals indicates the presence of an effective connection between them, and a white square implies that there is no effective connection between the two connected signals, both measured at 95% confidence level. For example, in Fig. 8 (a), signal 4 is influencing signal 5 (connected with a black square), and signal 5 is not influencing signal 3 (connected with a white square).

The GC results shown in Fig. 8 (b) are not very representative of the true EC between the 16 synthetic fNIRS signals (Fig. 8 (a)). The GC results depict many a false positives, and false negatives. An example of a false positive amongst GC results is signal 1 influencing signal 5 whereas signal 9 not influencing signal 10 is a false negative. The spurious results of GC indicate their inapplicability for the analysis of a network characterized by non-linear effective connections such as fNIRS signals.

In contrast, the results from the proposed third order E-FCM method are able to decode EC for 12 out of 16 signals (Fig. 8 (c)). For the case of E-FCM, a filled black square represents the acceptance of the t-test null hypothesis, $H_0$: The original and predicted signals connectivity values have the same mean at 95% confidence level. Table IV lists the p-values for the corresponding $H_0$ of E-FCM predicting signals based on its EC analysis of the 16 synthetic fNIRS signals.

### B. EC Computation on real fNIRS Data

The real fNIRS data [36] involving 27 surgeons (9 NVs, 10 TNs, and 8 EXs) performing a LS task is also used to assess the efficacy of the proposed method of a higher order E-FCM for delineating the underlying EC. In order to also better gauge the representation of oxy-Hb and deoxy-Hb in the resulting neuronal activity within the brain, the oxy-Hb and deoxy-Hb signals are simulated separately by the proposed E-FCM to compute their individual EC networks. The EC networks of the bi-dimensions of fNIRS signals are then used to generate an overall E-FCM.

The average error values (4) along with corresponding standard deviations comparing the accuracy in estimating

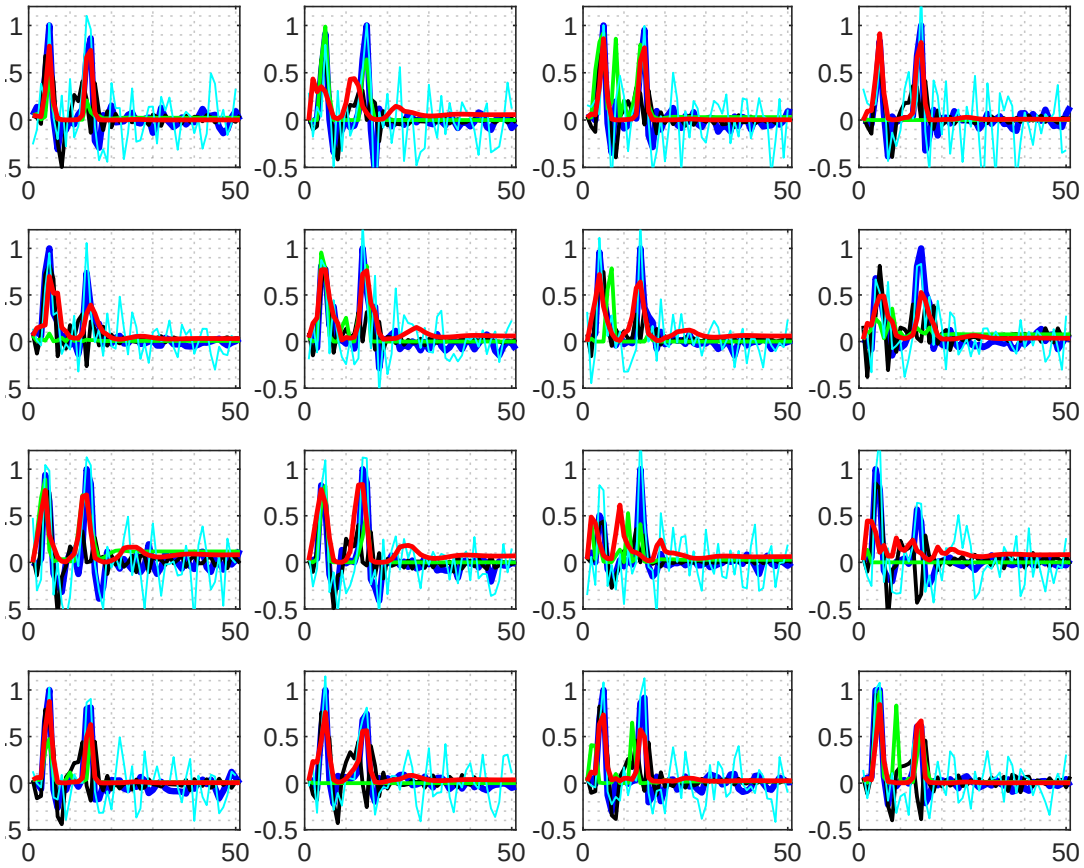

Fig. 7: Comparison of EC prediction results using proposed E-FCM (red) with original FCM (green), GC-AR (cyan), and DCM-GLM (black). The true EC are depicted in blue. On the x-axis are the values of time (sec), and y-axis has normalized amplitude of the synthetic fNIRS signals.

TABLE III: Error Values for GC-AR, DCM-GLM, original FCM, and third order E-FCM for 16 synthetic fNIRS signals.

| METHOD | ERROR | Signal No. 1 | 2 | 3 | 4 | 5 | 6 | 7 | 8 | 9 | 10 | 11 | 12 | 13 | 14 | 15 | 16 | AVG. ERROR |
|---|---|---|---|---|---|---|---|---|---|---|---|---|---|---|---|---|---|---|
| **GC-AR** | **Error 1** | 2.73 | 3.41 | 2.95 | 4.57 | **1.26** | 1.86 | **1.60** | **1.46** | 3.05 | 1.74 | 2.75 | 2.59 | 1.70 | 1.97 | 1.52 | **1.57** | 2.30 |
| | **Error 2** | 7.75 | 11.16 | 9.11 | 14.39 | 3.71 | 5.42 | **4.70** | **4.21** | 8.38 | 5.30 | 8.88 | 7.00 | 4.75 | 5.21 | 4.40 | 4.34 | 6.79 |
| **DCM-GLM** | **Error 1** | 2.81 | 2.52 | 2.65 | 2.48 | 1.84 | 2.26 | 1.61 | 3.44 | 3.05 | 2.98 | **1.27** | 2.57 | 3.20 | 3.05 | 3.09 | 2.67 | 2.59 |
| | **Error 2** | 9.10 | 8.00 | 9.01 | 8.61 | 5.92 | 7.70 | 5.66 | 10.44 | 8.45 | 8.82 | **4.13** | 7.23 | 9.80 | 9.23 | 9.78 | 7.99 | 8.12 |
| **FCM** | **Error 1** | **1.78** | **0.88** | 1.91 | 2.69 | 2.30 | **0.95** | 2.85 | 2.55 | 2.83 | **1.33** | 1.29 | 2.36 | **1.40** | 2.53 | 4.13 | 1.31 | 2.09 |
| | **Error 2** | **4.07** | **2.29** | 4.40 | 6.72 | 4.06 | **3.05** | 6.22 | 4.68 | 6.51 | 3.07 | 2.90 | 4.87 | 3.38 | 5.36 | 10.15 | 3.46 | 4.70 |
| **E-FCM** | **Error 1** | 4.37 | 2.92 | **0.99** | **1.89** | 1.40 | 1.40 | 2.88 | 2.11 | **2.08** | 1.54 | 3.14 | **0.36** | 1.72 | **1.38** | **1.09** | 1.64 | **1.93** |
| | **Error 2** | 9.10 | 4.44 | **2.55** | **4.85** | **2.53** | 3.42 | 5.26 | 4.33 | **4.67** | **3.00** | 5.62 | **0.68** | **2.48** | **2.32** | **2.44** | **2.46** | **3.76** |

TABLE IV: t-test Hypothesis and p-values for EC values of 16 synthetic fNIRS signals at 95% confidence level.

| t-TEST | Signal No. 1 | 2 | 3 | 4 | 5 | 6 | 7 | 8 |
|---|---|---|---|---|---|---|---|---|
| **t-test h** | 0 | 0 | 0 | 0 | 0 | 0 | 0 | 0 |
| **t-test p** | 0.86 | 0.05 | 0.55 | 0.38 | 0.43 | 0.06 | 0.14 | 0.58 |
| | **9** | **10** | **11** | **12** | **13** | **14** | **15** | **16** |
| **t-test h** | 1 | 1 | 1 | 1 | 0 | 0 | 0 | 0 |
| **t-test p** | 0.04 | 0.01 | 0.02 | 0.02 | 0.43 | 0.25 | 0.50 | 0.85 |

Significance Level $\alpha = 0.05$, h=0 denotes $H_0$ is accepted.
t-test accepts $H_0$ for 12/16 signals.

fuzzy effective connections between oxy-Hb and deoxy-Hb by proposed third order E-FCM are listed in Table V. Essentially, hemoglobin group E-FCM simulation for which the average error is greater, its weights are scaled down by the corresponding percentage hence taking forward more of the accurate EC estimates to contribute to the combined E-FCM. For example, for NVs, the oxy-Hb weights are scaled down by 3.1% before mapping into the overall E-FCM.

In order to assess the third order E-FCM results for statistical significance, Table A.1 lists the number of the t-test $H_0$ being accepted for all subjects of category NVs, TNs, and EXs. The null hypothesis is defined as $H_0$: The original and predicted signals connectivity values have the same mean

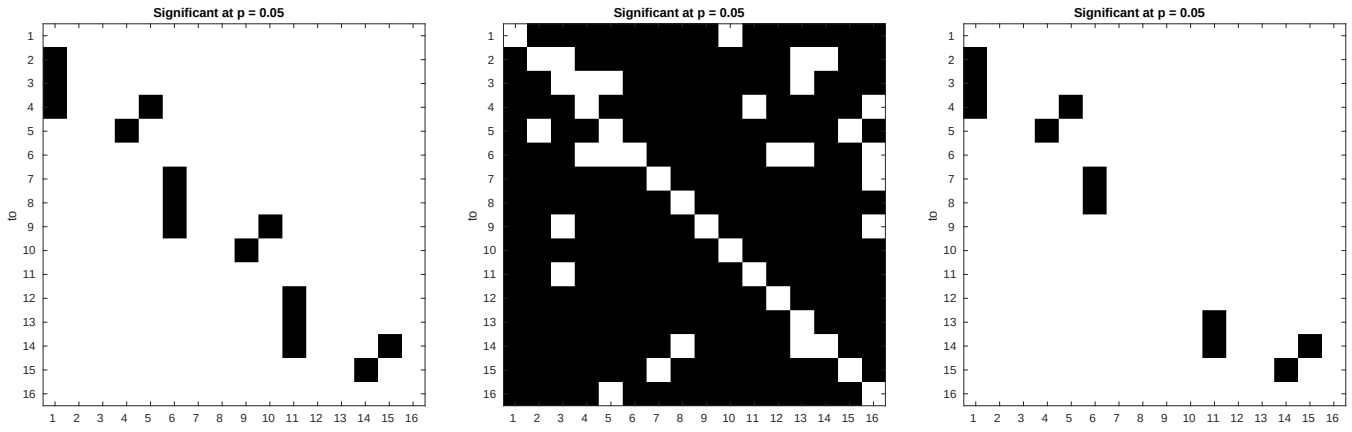


(a) True causal relation (b) GC Result (c) E-FCM Result

Fig. 8: Comparison of EC estimation for 16 synthetic fNIRS using GC (b), and 3rd order E-FCM (c), with the true effective connections (a).

TABLE V: Average Error Values for Oxy-Hb and Deoxy-Hb fNIRS simulation by 3rd order E-FCM

| | **Novices (NVs)** | **Trainees (TNs)** | **Experts (EXs)** |
|---|---|---|---|
| **Oxy-Hb** | 120.25 $\pm$ 29.85 | 122.79 $\pm$ 32.89 | 156.38 $\pm$ 46.52 |
| **Deoxy-Hb** | 116.62 $\pm$ 27.14 | 119.99 $\pm$ 43.44 | 125.49 $\pm$ 73.45 |
| **Error** | Oxy-Hb by 3.1% | Oxy-Hb by 2.3% | Oxy-Hb by 19.8% |

Mean Error 1 (4) of all subjects with standard deviations are presented.

at 95% confidence level. The results indicate that for most of the channels, across all subjects and expertise levels, the $H_0$ is accepted indicating the prowess of the proposed higher order E-FCM for delineating the EC in fNIRS data. However, the results in Table A.1 indicate that underlying effective connections in oxy-Hb results are better understood by the proposed third order E-FCM in comparison to the deoxy-Hb for less experienced subjects. However, the accuracy of the predicted signals, for both oxy-Hb and deoxy-Hb signals, can also be seen to decline as the expertise level increases. This could perhaps be owing to changes in the memory order of the EC of the underlying channels on account of increased experience but needs further investigation since, in this work, the order of the E-FCM model is not varied with the change in expertise level.

In order to facilitate the comparison of brain network evolution as an individual gains a certain degree of expertise in doing a certain task, LS in this case, Fig. A.1 shows a plot of the E-FCMs generated from oxy-Hb and deoxy-Hb fNIRS signals along with corresponding combined E-FCM for NVs, TNs, and EXs. Please note only the most significant connections are shown in Fig. A.1 which have fuzzy degrees of relationship greater than 90th percentile. A noteworthy observation that can be made from Fig. A.1 is that as the expertise level increases, the number of significant EC (strength of fuzzy degrees of relationship greater than 90th percentile) is more for deoxy-Hb E-FCMs as compared to oxy-Hb E-FCMs signifying that perhaps deoxy-Hb signals hold more latent information with regards to channels underlying EC as compared to oxy-Hb signals if the brain networks have evolved owing to more experience. The quiescent EC structure within the deoxy-Hb signals for more experienced subjects could also explain why a greater number of t-test $H_0$ got rejected in Table A.1 against corresponding oxy-Hb channels.

## VI. Neuropsychological discussion

In this work the real fNIRS data [36] used in Experiment 2 entailed subjects which differed in their level of expertise for performing a pre-defined LS task. The fNIRS data recorded, whilst the subjects performed LS task, is consequently used to assess the efficacy of the novel, high order and regularized E-FCM method presented. In this section, the results obtained for EC between ROIs from the proposed third order E-FCM model are gauged against similar works in the literature.

The results from third order E-FCM model indicate network connections change from random activations to evenly spread out along with more positive influences as the expertise level increase as shown in Fig. A.1. This is in agreement with the current findings [35] [36] that as an individual progress in learning, their brain networks evolve and optimize their connections. Another perspective for underpinning the EC analysis in between ROIs is done by collapsing the weights according to PFC and MC as shown in Fig. 9. This is done by first averaging the weights for all subject's oxy-Hb and deoxy-Hb of a given expertise level, and consequently finding the mean of the average values for the individual hemoglobin's ROIs weights. The resultant averaged values are then scaled to unit length for each connection i.e. PFC to PFC, PFC to MC, MC to PFC, and MC to MC across the three expertise level. A similar trend can also be seen in Fig. 9, with NVs relying more on inter PFCs and almost non-dependent on MCs connections as compared to TNs and EXs. TNs and EXs rely more on inter MC connections and less on inter PFC with progression towards a balanced corroboration between ROIs

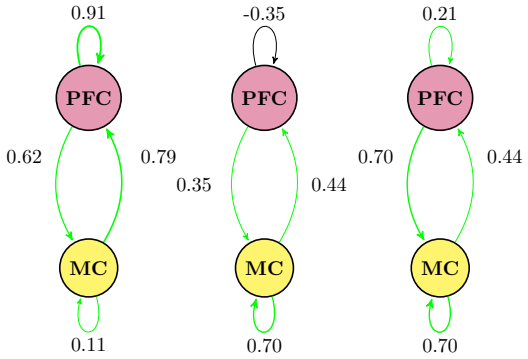


Fig. 9: EC strength between ROIs: PFC and MC for NVs (left), TNs (center), and EXs (right).

as more experience is gained hence spreading the cognitive load in contrast to NVs [35] [36]. This progression trend with increased experience is also intercepted well by third order E-FCM as can be seen in Fig. A.1 with more strong positive cause-effect relations between PFC and MC for TNs and EXs as compared to NVs.

The shift in brain activations from PFC to MC on account of increased experience is also in line with the findings from the work of Sanes [52] which observed a decrease in EC in frontal pathway encompassing the regions of inferior frontal gyrus and precentral gyrus brain as a particular visual-motor coupled task is learnt. Another distinct work by Kawai *et al.* [53] focusing on the particular role that MC takes whilst a certain task is learnt concludes that MC is critical for learning of a task but not essential for execution of a previously learnt motor task. They conclude that MC engages subcortical motor cortex circuits upon learning of a task and assigns them the execution of the learnt task. This frees the MC for any new learning activity and is in coherence with the findings of this work that brain networks evolve to a more balanced configuration, on acquisition of a certain level of expertise, without draining any particular segment of the brain.

The work by Chersi *et al.* [54] also report a similar trend of high dependency on PFC when the subject is inexperienced with the task undertaken and with more experience internal brain areas such as basal ganglia (BG) are more activated. The task carried out by the animal in the study [54] was to switch on flashing lights by pressing corresponding buttons. Once the animal learnt the task, the button and flashing light sequence is changed so as to coerce it to suppress its learnt behaviors. The study concluded that PFC regions are more involved during the learning of a task whereas BG takes over when a goal directed behavior is required.

## VII. Conclusions and Future Work

This work has demonstrated a novel approach to identify EC connections between fNIRS data using enhanced higher order E-FCM model. The significance of accurately deciphering EC from fNIRS data is paramount for the advancement of research in the working and evolution of the human brain. In this regard, the combination of a higher order E-FCM offers a novel, more robust, and fully automated solution for uncovering the EC networks between fNIRS data. The strength of the proposed model is shown by its superior accuracy in identifying the effective connections for both synthetic and real fNIRS data at 95% confidence level.

The improvements in FCM framework, along with tuning of the transformation function parameter, renders the proposed higher order E-FCM more adaptable to the requirements of a given complex network. An attempt is also made to study the individual significance of oxy-Hb and deoxy-Hb signals while uncovering the underlying EC within the fNIRS signals. The EC networks determined from individual oxy-Hb and deoxy-Hb E-FCMs are used in conjunction in a novel approach to arrive at a combined E-FCM representing the characteristics from both dimensions of fNIRS signals. The preliminary results are in line with the current literature that the dual dimension of fNIRS data are independent however deoxy-Hb signals might be able to identify more effective relations based on greater number of significant EC connections in Fig. A.1 as compared to oxy-Hb signals. Likewise, in Table A.1, the number of signals for which the t-test $H_0$ is accepted is greater for oxy-Hb signals with lesser experience (NVs: $H_0 = 144$, TNs: $H_0 = 140$ , EXs: $H_0 = 102$) than that for deoxy-Hb signals with greater experience (NVs: $H_0 = 131$, TNs: $H_0 = 141$ , EXs: $H_0 = 111$) implying the presence of a more latent EC information in deoxy-Hb signals, which becomes more pronounced with an increase in experience, that was not detected by the proposed fixed higher order E-FCM model. The novel finding of deoxy-Hb signals becoming more representative of the underlying EC as an individual gains experience in a certain motor task may help to understand the evolution of brain networks on acquisition of experience.

The future work aims at exploring the effect of modifying the order of the E-FCM model as the expertise level increases. This can be of significance because as the brain networks evolve the memory order of the underlying EC in brain network may also increase or decrease. This needs to be further investigated but an intuitive hypothesis can be that optimization of brain networks would have a bearing on the memory order of EC within the ROIs.

## References

[1] A. Aertsen and H.Preissl, "Dynamics of activity and connectivity in physiological neuronal networks," *Nonlinear Dynamics and Neuronal Networks*, 1991.

[2] K. J. Friston, "Functional and effective connectivity: A review," *Brain Connectivity*, vol. 1, no. 1, pp. 13–36, 2011.

[3] R. Parasuraman and G. F. Wilson, "Putting the brain to work: Neuroergonomics past, present, and future," *Human Factors:The Journal of the Human Factors and Ergonomics Society*, vol. 50, no. 3, p. 468–474, 2008.

[4] K. J. Friston, "Causal modelling and brain connectivity in functional magnetic resonance imaging," *PLoS Biol*, vol. 7, 2009.

[5] S. Tak, A. Kempn, K. Friston, A. Leff, and W. Penny, "Dynamic causal modelling for functional near-infrared spectroscopy," *NeuroImage*, vol. 111, pp. 338–349, 2015.

[6] L. Helmut, *Econometric analysis with vector autoregressive models*. Wiley, 2007.

[7] M. Eichler, *Causal inference in time series analysis*. Wiley, 2012.

[8] G. Stephanie, "Limitations of granger causality analysis to assess the price effects from the financialization of agricultural commodity markets under bounded rationality," *Institute for Food and Resource Economics*, 2012.

[9] J. D. Hamilton, *Time series analysis*. Princeton, 1994.

[10] B. Kosko, *Neural Network and Fuzzy Systems*. Prentice-Hall, 1992.

[11] D. Hakan, H. Hagras, and V. Callaghan, "Intelligent association selection of embedded agents in intelligent inhabited environments," *Pervasive and Mobile Computing*, vol. 3, pp. 117–157, 2012.

[12] P. Hanafizadeh and R. Aliehyaei, "The application of fuzzy cognitive map in soft system methodology," *Systemic Practice and Action Research*, vol. 24, pp. 325–354, 2011.

[13] B. Kosko, "Fuzzy cognitive maps," *Int. J of Man-Machine Studies*, vol. 24, pp. 65–75, 1986.

[14] W. Stach, L. Kurgan, W. Pedrycz, and M. Reformat, "Genetic learning of fuzzy cognitive maps," *Fuzzy Sets and Systems*, vol. 153, pp. 371–401, 2005.

[15] W. Stach, L. Kurgan, and W. Pedrycz, "Higher-order fuzzy cognitive maps," *NAFIPS*, 2006.

[16] J. Aguilari, "A survey about fuzzy cognitive maps papers," *Int. J. of Computational Cognition*, vol. 3, pp. 27–33, 2005.

[17] E. I. Papageorgiou and W. Froelich, "Application of evolutionary fuzzy cognitive maps for prediction of pulmonary infections," *IEEE Transactions on information technology in biomedicine*, vol. 16, pp. 143–149, 2011.

[18] A. N. Averkin and S. A. Kaunov, "Regularization of fuzzy cognitive maps for hybrid decision support system," *RSFDGrC*, vol. 6743, pp. 139–146, 2011.

[19] S. Bueno and J. L. Salmeron, "Benchmarking main activation functions in fuzzy cognitive maps," *Expert Systems with Applications*, vol. 36, pp. 5221–5229, 2009.

[20] L. Holper, F. Scholkmann, and M. Wolf, "Between-brain connectivity during imitation measured by fnirs," *NeuroImage*, vol. 63, pp. 212–222, 2012.

[21] C. H. Im, Y. J. Jung, S. Lee, D. Koh, D. Kim, and B. M. Kim, "Estimation of directional coupling between cortical areas using near-infrared spectroscopy(nirs)," *Optical Society of America, Medical optics and biotechnology*, vol. 18, pp. 5730–5739, 2010.

[22] S. Bajaj, D. Drake, A. J. Butler, and M. Dhamala, "Oscillatory motor network activity during rest and movement: an fnirs study," *Frontiers in System Neuroscience*, 2014.

[23] Z. Yuan, "Combining independent component analysis and granger causality to investigate brain network dynamics with fnirs measurements," *Biomedical Optics Express*, vol. 4, pp. 2629–2643, 2013.

[24] S. Yang and J. Liu, "Time-series forecasting based on high-order fuzzy cognitive maps and wavelet transform," *IEEE TFS*, vol. 26, pp. 3391–3402, 2018.

[25] X. Zou and J. Liu, "A mutual information-based two-phase memetic algorithm for large-scale fuzzy cognitive map learning," *IEEE TFS*, vol. 26, pp. 2120 – 2134, 2017.

[26] K. Wu and J. Liu, "Learning large-scale fuzzy cognitive maps based on compressed sensing and application in reconstructing gene regulatory networks," *IEEE TFS*, vol. 25, pp. 1546 – 1560, 2017.

[27] ——, "Robust learning of large-scale fuzzy cognitive maps via the lasso from noisy time series," *Knowledge-Based Systems*, vol. 113, pp. 23–38, 2016.

[28] J. Liu, Y. Chi, and C. Zhu, "A dynamic multiagent genetic algorithm for gene regulatory network reconstruction based on fuzzy cognitive maps," *IEEE TFS*, vol. 24, pp. 419 – 431, 2015.

[29] S. Tang and J. Han, "A pruning based method to learn both weights and connections for lstm," 2015.

[30] N. Srivastava, G. Hinton, A. Krizhevsky, I. Sutskever, and R. Salakhutdinov, "Dropout: A simple way to prevent neural networks from overfitting," *Journal of Machine Learning Research*, vol. 15, pp. 1929–1958, 2014. [Online]. Available: http://jmlr.org/papers/v15/srivastava14a.html

[31] L. Wan, M. Zeiler, S. Zhang, Y. L. Cun, and R. Fergus, "Regularization of neural networks using dropconnect," vol. 28, 2013, pp. 1058–1066. [Online]. Available: http://proceedings.mlr.press/v28/wan13.html

[32] F. Scarpa, S. Brigadoi, S. Cutini, P. Scatturin, M. Zorzi, R. Dell'Acqua, and G. Sparacino, "A reference-channel based methodology to improve estimation of event-related hemodynamic response from fnirs measurements," *NeuroImage*, vol. 72, pp. 106–119, 2013.

[33] N. D. Tam and G. Zouridakisb, "Temporal decoupling of oxy- and deoxy-hemoglobin hemodynamic responses detected by functional near-infrared spectroscopy (fnirs)," *Journal of Biomedical Engineering and Medical Imaging*, vol. 1, 2014.

[34] J. Andreu-Perez, F. Cao, H. Hagras, and G. Z. Yang, "A self-adaptive online brain machine interface of a humanoid robot through a general type-2 fuzzy inference system," *IEEE Transactions on Fuzzy Systems*, vol. 26, pp. 101 – 116, 2016.

[35] M. Kiani, J. Andreu-Perez, D. R. Leff, A. Darzi, and G. Z. Yang, "Shedding light on surgeons' cognitive resilience: A novel method of topological analysis for brain networks," *The Hamlyn Symposium on Medical Robotics*, p. 55, 2014.

[36] J. Andreu-Perez, D. R. Leff, K. Shetty, A. Darzi, and G.-Z. Yang, "Disparity in frontal lobe connectivity on a complex bimanual motor task aids in classification of operator skill level," *Brain Connectivity*, vol. 6, 2016.

[37] A. F. Abdelnour and T. Huppert, "Real-time imaging of human brain function by near-infrared spectroscopy using an adaptive general linear model," *Neuroimage*, vol. 46, pp. 133–143, 2009.

[38] G. H. Glover, "Deconvolution of impulse response in event-related bold fmri," *Neuroimage*, vol. 9, pp. 416–429, 1999.

[39] M. Izzetoglu, P. Chitrapu, S. Bunce, and B. Onaral, "Motion artifact cancellation in nir spectroscopy using discrete kalman filtering," *BioMedical Engineering OnLine*, 2010.

[40] L. Luo, W. Liu, I. Koprinska, and F. Chen, "Discovering causal structures from time series data via enhanced granger causality," *Advances in Artificial Intelligence*, vol. 9457, pp. 365 – 378, 2015.

[41] A. R. Laird, J. L. Robinson, K. M. McMillan, D. Tordesillas-Gutierrez, and S. T. Moran, "Comparison of the disparity between talairach and mni coordinates in functional neuroimaging data: Validation of the lancaster transform," *Neuroimage*, vol. 51, pp. 677–683, 2010.

[42] J. L. Lancaster, M. G. Woldorff, L. M. Parsons, M. Liotti, C. S. Freitas, L. Rainey, P. V. K. D. Nickerson, S. A. Mikiten, and P. T. Foxm, "Automated talairach atlas labels for functional brain mapping," *Human Brain Mapping*, vol. 10, pp. 120–131, 2000.

[43] N. D. Tam and G. Zouridakis, "Differential temporal activation of oxy- and deoxy-hemodynamic signals in optical imaging using functional near-infrared spectroscopy (fnirs)," *BMC Neuroscience*, vol. 16, 2015.

[44] I. Tachtsidis and F. Scholkmann, "False positives and false negatives in functional near-infrared spectroscopy: issues, challenges, and the way forward," *Neurophotonics*, vol. 3, 2016.

[45] S. Sasai, F. Homae, H. Watanabe, and G. Taga, "Frequency-specific functional connectivity in the brain during resting state revealed by nirs," *NeuroImage*, vol. 56, pp. 252–257, 2011.

[46] E. I. Papgeorgiou, "Learning algorithms for fuzzy cognitive maps - a review study," *IEEE Transactions of Systems, Man, and Cybernetics*, vol. 42, pp. 150–163, 2011.

[47] K. J. Friston, A. P. Holmes, K. J. Worsley, J.-B. Poline, C. D. Frith, and R. S. J. Frackowiak, "Statistical parametric maps in functional imaging: A general linear approach," *Hum. Brain Mapp*, vol. 2, p. 189–210, 1995.

[48] R. Henson and K. Friston, *Statistical Parametric Mapping: The Analysis of Functional Brain Images, Chapter 14. Convolution Models for fMRI*. Academic Press, 2007.

[49] C. W. Granger, "Investigating causal relations by econometric models and cross-spectral methods," *Econometrica: Journal of the Econometric Society*, vol. 37, pp. 424–438, 1969.

[50] A. K. Seth, "Matlab toolbox for granger causal connectivity analysis," *Journal of neuroscience methods*, vol. 186, pp. 262–273, 2010.

[51] U. C. L. Wellcome Trust Centre for Neuroimaging, "SPM software," http://www.fil.ion.ucl.ac.uk/spm/, [Online; accessed 10-Oct-2019].

[52] J. N. Sanes, "Neocortical mechanisms in motor learning," *Current Opinion in Neurobiology*, vol. 13, pp. 225–231, 2003.

[53] R. Kawai, T. Markman, R. Poddar, A. L. F. R. Ko, A. K. Dhawale, A. R. Kampff, and B. P. Olveczky, "Motor cortex is required for learning but not for executing a motor skill," *Neuron*, vol. 86, pp. 800–812, 2015.

[54] F. Chersi, M. Mirolli, G. Pezzulo, and G. Baldassarre, "A spiking neuron model of the cortico-basal ganglia circuits for goal-directed and habitual action learning," *Neural Networks*, vol. 41, pp. 212–224, 2013.

# APPENDIX

TABLE A.1: Percentage ratio of No. of t-Test $H_0$ accepted to No. of Subjects (N), $^{H_0}/_N$ , for oxy-Hb and deoxy-Hb of 9 NVs, 10 TNs, and 8 EXs at 95% confidence level

| | $\mathbf{H_0/N}$ | | | | | |
|---|---|---|---|---|---|---|
| **Channel No.** | **NVs Oxy-Hb** | **NVs Deoxy-Hb** | **TNs Oxy-Hb** | **TNs Deoxy-Hb** | **EXs Oxy-Hb** | **EXs Deoxy-Hb** |
| **1** | 100.0% | 88.9% | 90.0% | 90.0% | 87.5% | 75.0% |
| **2** | 100.0% | 100.0% | 90.0% | 90.0% | 87.5% | 100.0% |
| **3** | 100.0% | 100.0% | 100.0% | 100.0% | 100.0% | 87.5% |
| **4** | 100.0% | 88.9% | 80.0% | 90.0% | 75.0% | 87.5% |
| **5** | 100.0% | 77.8% | 100.0% | 100.0% | 62.5% | 87.5% |
| **6** | 100.0% | 100.0% | 90.0% | 80.0% | 75.0% | 100.0% |
| **7** | 100.0% | 77.8% | 90.0% | 100.0% | 62.5% | 75.0% |
| **8** | 100.0% | 100.0% | 70.0% | 80.0% | 87.5% | 100.0% |
| **9** | 100.0% | 100.0% | 90.0% | 100.0% | 75.0% | 87.5% |
| **10** | 100.0% | 100.0% | 90.0% | 80.0% | 87.5% | 87.5% |
| **11** | 100.0% | 88.9% | 90.0% | 90.0% | 100.0% | 100.0% |
| **12** | 100.0% | 77.8% | 100.0% | 80.0% | 50.0% | 62.5% |
| **13** | 100.0% | 88.9% | 70.0% | 80.0% | 87.5% | 75.0% |
| **14** | 100.0% | 88.9% | 80.0% | 70.0% | 87.5% | 87.5% |
| **15** | 100.0% | 88.9% | 90.0% | 90.0% | 87.5% | 87.5% |
| **16** | 100.0% | 88.9% | 80.0% | 90.0% | 62.5% | 87.5% |

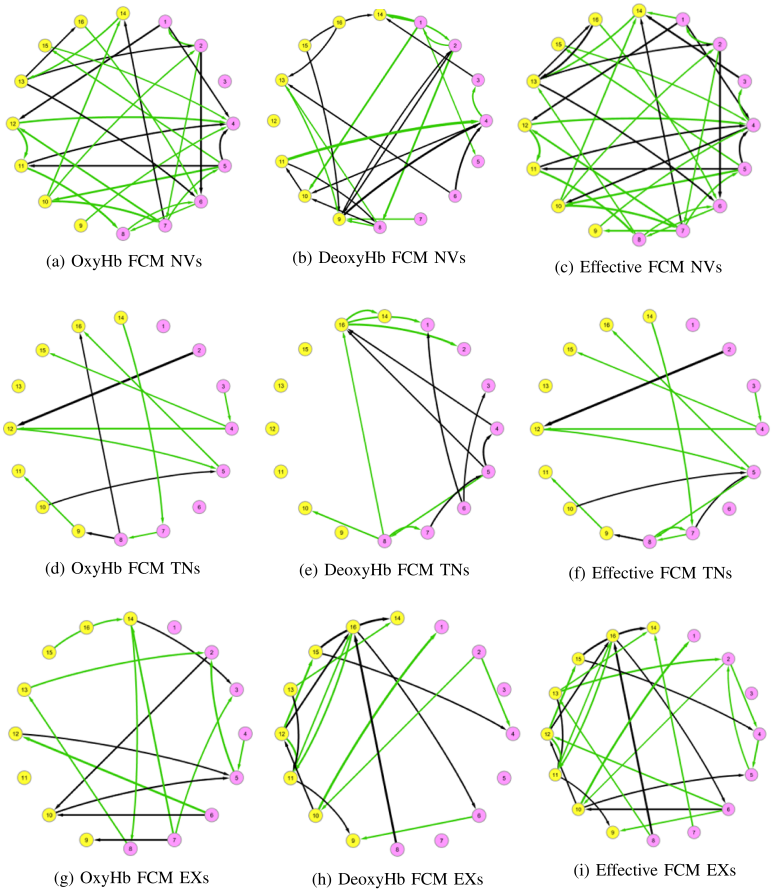

(a) OxyHb FCM NVs (b) DeoxyHb FCM NVs (c) Effective FCM NVs

(d) OxyHb FCM TNs (e) DeoxyHb FCM TNs (f) Effective FCM TNs

(g) OxyHb FCM EXs (h) DeoxyHb FCM EXs (i) Effective FCM EXs

Fig. A.1: Averaged oxy-Hb and deoxy-Hb E-FCMs with combined E-FCMs for Novices (NVs), Trainees (TNs), and Experts (EXs). The signals in PFC region are annotated in pink, and those in MC are in yellow. A green line signifies presence of a positive causal interaction between the connecting signals, and the presence of a black line denotes a negative causal interaction between the connecting signals.